Eliassen-Palm Fluxes of the Diurnal Tides from the Whole Atmosphere Community Climate Model-Extended (WACCM-X)

McArthur "Mack" Jones Jr.

Academic Affiliation, Fall 2009: Senior, Millersville University

SOARS® Summer 2009

Science Research Mentors: Han-Li Liu and Arthur Richmond
Writing and Communications Mentor: Jamaica Jones
Computer Mentor: Joe McInerney

ABSTRACT

[1] Through perturbation interactions with the zonal mean flow, the migrating diurnal tide and the diurnal eastward 3 (DE3) tide are fundamental to a holistic understanding of the atmospheric dynamics at mesosphere lower thermosphere (MLT) and low ionospheric altitudes. Previous tidal studies have noted the semiannual variability associated with the migrating diurnal tide and the DE3 tide, which maximize around equinox and minimize around solstice. Seasonally varying source and dissipation regions and/or wind structures are believed to cause the differences in the maximum amplitudes experienced between the two equinoxes. Utilizing monthly averaged output from the Whole Atmosphere Community Climate Model-Extended (WACCM-X), this study is among the first to apply this model to a diagnostic examination of the sources and sinks of tidal momentum and document the associated seasonal variability. From the averaged amplitudes obtained during March and September, the WACCM-X replicates the observed seasonal variability associated with the migrating diurnal tide and the DE3 tide. Calculating the divergence of the Eliassen-Palm Flux (EP Flux) for the migrating diurnal tide revealed robust seasonal variation which may be linked to differential solar heating of ozone in the stratosphere. Seasonal variation in the tropospheric sources of the DE3 tidal momentum alone does not appear to explain the semiannual variability observed in the tidal amplitudes. This study provides a better understanding of the seasonal variation in the generation and dissipation mechanisms of the migrating diurnal tide and the DE3 tide.

The Significant Opportunities in Atmospheric Research and Science (SOARS) Program is managed by the University Corporation for Atmospheric Research (UCAR) with support from participating universities. SOARS is funded by the National Science Foundation, the National Oceanic and Atmospheric Administration (NOAA) Climate Program Office, the NOAA Oceans and Human Health Initiative, the Center for Multi-Scale Modeling of Atmospheric Processes at Colorado State University, and the Cooperative Institute for Research in Environmental Sciences. SOARS is a partner project with Research Experience in Solid Earth Science for Student (RESESS).

1. Introduction

[2] Atmospheric tides are dynamical perturbations of temperature, wind, pressure, and density, with frequencies that are harmonics of a solar or lunar day [*Chapman and Lindzen*, 1970; *Forbes* 1995; *Hagan et al.,* 2001]. Solar atmospheric tides are generated from the regular daily variation of solar heating [*Volland,* 1988]. These thermally forced tides owe their existence to the absorption of this spatially nonuniform solar radiation by a suite of atmospheric constituents, which includes water vapor (H_2O), absorption of infrared (IR) radiation, stratospheric and mesospheric ozone (O_3) absorption of ultraviolet (UV) radiation, and thermospheric oxygen absorption of extreme ultraviolet radiation (EUV) [*Andrews et al.,* 1987, *Pancheva et al.,* 2009]. Other forcing mechanisms include latent heat release from convective processes within the upper troposphere, nonlinear interactions with planetary waves, and variations in sea-land topography.

[3] The propagation of atmospheric tides is central to the dynamics of the mesosphere lower thermosphere (MLT) and low altitude ionosphere, which contains charged particles due to the solar ionization of atmospheric molecules. Consequently, tidal propagation through the MLT and ionospheric region causes deviations in wind and temperature fields. Specifically, these variations in lower thermospheric winds can be responsible for perturbations in the Earth's magnetic field and for driving the ionospheric dynamo [*Maeda, 1968; Richmond and Roble,* 1987; *Richmond,* 1995]. This ionospheric dynamo acts to convert kinetic energy into electric energy, which in turn drives electric currents and electric fields that subsequently change the ionospheric density [*Kelley, 1989*].

[4] Even today, the ionosphere remains the largest error source of GPS navigation [*Coster and Komjathy,* 2008]. For example, difficulties encountered by radio communications, GPS, and Differential GPS (DGPS) users are attributed to variations in electron density throughout the ionosphere. Furthermore, anomalies in electron densities occasionally interfere with the Department of Defense's precision navigation and strike operations [*Coster and Komjathy,* 2008, *American Meteorological Society,* 2008]. Radio communication is dependent upon electron density, as electromagnetic waves can experience changes in propagation direction due to gradients in electron density [*Dabas,* 2000]. Given that atmospheric tides are a prominent dynamical feature in the MLT and ionospheric region, further understanding of their sources and sinks is essential when considering middle to upper atmospheric dynamics.

[5] Thermally forced atmospheric tides can be classified into migrating (sun-synchronous) or nonmigrating tides. Migrating tides are a global-scale feature, propagating westward with the apparent motion of the sun [*Pancheva et al.,* 2009; *Hagan et al.,* 2001]. Typically, migrating tides are forced mainly in the troposphere and stratosphere, from which they propagate vertically into the MLT region [*Forbes* 1995]. Once reaching MLT altitudes, thermally forced tides are capable of attaining large amplitudes due to decreased density (conservation of energy), thereby leading to the aforementioned anomalies in MLT wind and temperature fields [*Volland,* 1988]. Because it is the largest tidal component in the MLT region, the migrating diurnal tide, which has a period of 24 h and a zonal wave number of –1 (negative sign refers to the westward propagation), will be one tidal component of interest for this research [*Forbes* 1995].

[6] Although, the migrating diurnal tide propagates westward, eastward components of tides are also generated due to the nonuniformity of the sources and the nonlinearity of the atmosphere. Because these eastward components deviate from the apparent motion (westward)

of the sun they are classified as nonmigrating tides. Nonmigrating tides are evidently forced by latent heat release, nonlinear interaction between the migrating diurnal tide and/or planetary waves [*Wu et al,* 2008b, *Hagan and Forbes*, 2002, 2003]. Specifically, the eastward propagating zonal wave number 3 diurnal tide (DE3) will be the other tidal component of interest for this research as it, too, can realize large amplitudes in the MLT region.

[7] Numerical model output such as MLT winds, temperature, and pressure fields aids in resolving a representative global portrayal of the diurnal tides, and provides a means to develop a greater understanding of their sources and sinks, seasonal variability, and the effects of MLT dynamics. The Whole Atmosphere Community Climate Model-Extended (WACCM-X), so called because the model extends from the surface of the earth to roughly 500 km, provides the data output necessary to simulate these variations in the diurnal tides. As one of the initial tidal analyses to utilize the WACCM-X, this study notes that by extending the model to the upper thermosphere (~500 km), scientists are now better able to replicate these tides in the MLT region [*Liu et al.*, manuscript in preparation, 2009].

[8] *Vincent et al.*, [1989], *Hays et al.*, [1994], *Chang et al.*, [2008], and *Wu et al*, [2008 a,b] all note the semiannual fluctuation in the amplitude of the migrating diurnal tide and DE3. The migrating diurnal tide normally maximizes around equinox (March/September) and minimizes around solstice (June/December), because during equinox, the heating over the Earth is more symmetric with respect to the equator, thereby providing the optimal forcing conditions. In the case of migrating diurnal tide, the maximum amplitude observed in March is greater than that observed in September, as displayed below in Figure 1 [*Chang et al.*, 2008]. Conversely, the DE3 generally experiences a greater peak in September than in March [*Wu et al,* 2008b]. Figure 2 is consistent with the previous statement, revealing a marginally higher maximum in September when compared to March.

[9] *Hays et al.*, [1994] suggests the seasonal modulation in amplitude of the migrating diurnal tide may be caused by a variation in sources at tropospheric altitudes. *Wu et al*, [2008b] concluded that interannual variability observed in the DE3 warrants additional investigation. Therefore, the question remains whether the seasonal fluctuation of the diurnal tides is associated with seasonally varying sources of momentum and/or heat. This research further examines this issue by using WACCM-X output from March and September of a one-year run to diagnostically investigate the difference between the amplitudes observed.

[10] Calculating the Eliassen-Palm Flux (EP Flux), which computes zonal mean flow-wave interaction, allowed us to better diagnose and thus document the sources and sinks of momentum during the March and September equinoxes [*Andrews et al.*, 1987]. This in turn provided a basis from which we quantified the difference in the amplitudes observed [*Andrews et al.*, 1987]. Ultimately, this research supplies additional understanding into the seasonal variation associated with atmospheric tides.

[11] Section 2 presents a more in-depth description of the WACCM-X and the data used for this study. Section 3 offers supplementary mathematical information regarding the EP Flux and how it was computed given our data set. Section 4 and 5 documents of the semiannual variability associated with the migrating diurnal tide and the DE3 tide sources and sinks of tidal momentum. Section 6 provides a brief summary and poses future research questions.

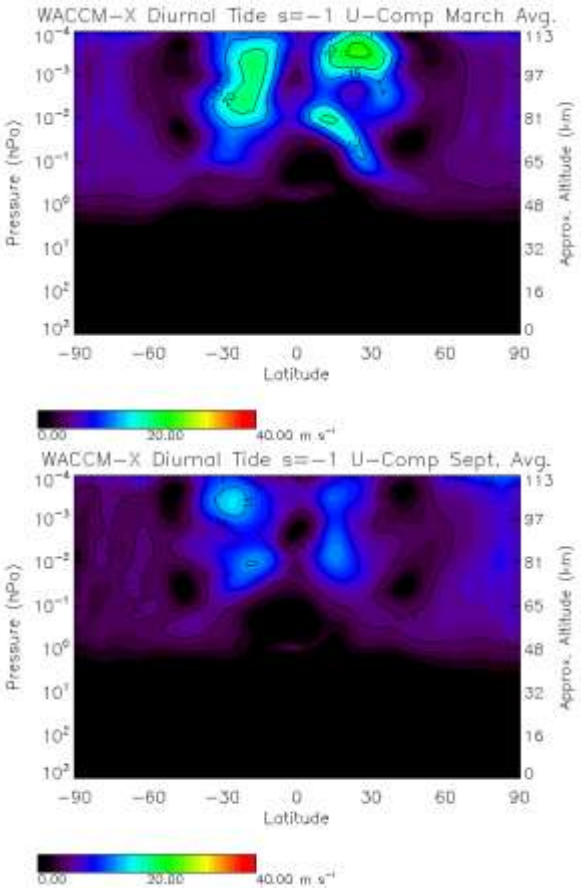
WACCM−X Diurnal Tide s=−1 U−Comp March Avg.
Pressure (hPa)
Approx. Altitude (km)
Latitude
−90 −60 −30 0 30 60 90
0.00 20.00 40.00 m s⁻¹
WACCM−X Diurnal Tide s=−1 U−Comp Sept. Avg.
Pressure (hPa)
Approx. Altitude (km)
Latitude
−90 −60 −30 0 30 60 90
0.00 20.00 40.00 m s⁻¹

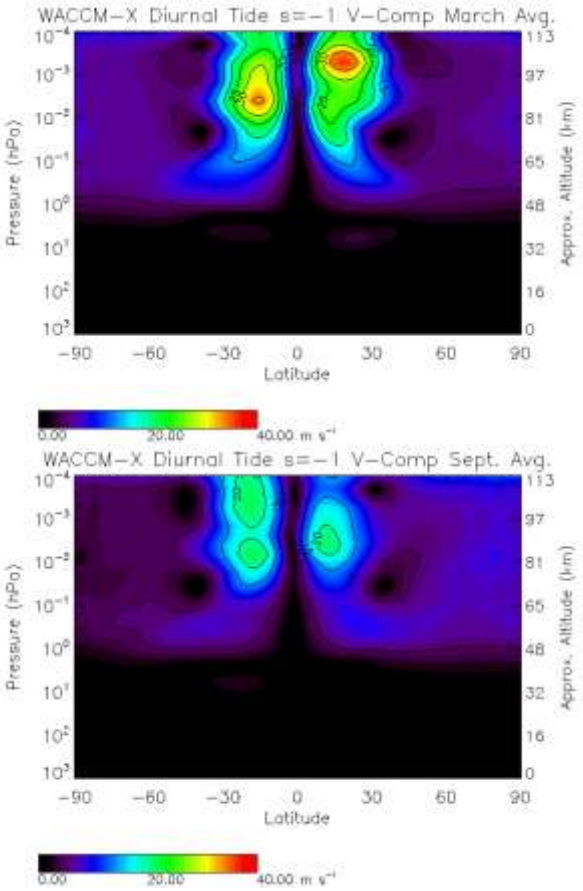
WACCM–X Diurnal Tide s=–1 V–Comp March Avg.
Pressure (hPa)
Approx. Altitude (km)
Latitude
WACCM–X Diurnal Tide s=–1 V–Comp Sept. Avg.
Pressure (hPa)
Approx. Altitude (km)
Latitude
0.00
20.00
40.00 m s⁻¹

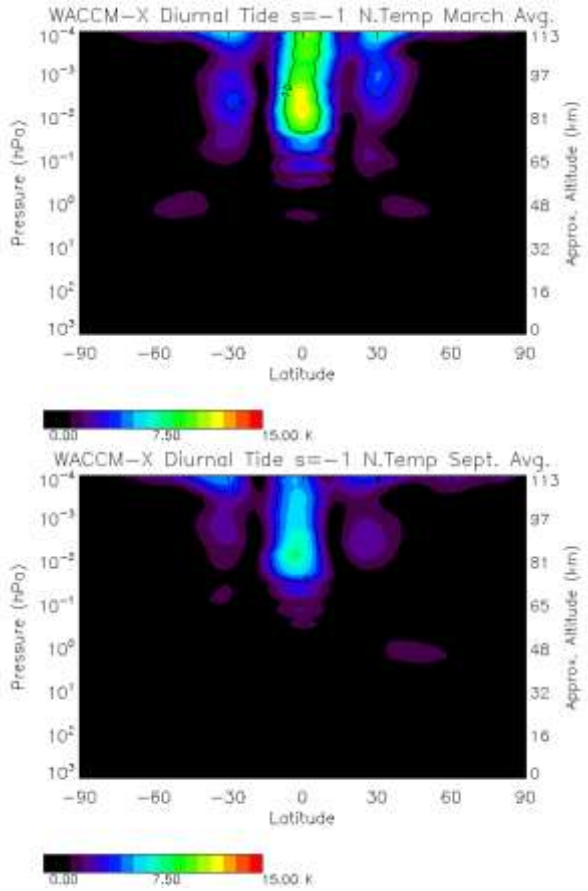

Figure 1. The migrating diurnal tide monthly average amplitudes from March (left) and September (right) of the zonal wind (top), meridional wind (middle), and temperature (bottom). Wind contours of 5 m/s, temperature contours of 5 K.

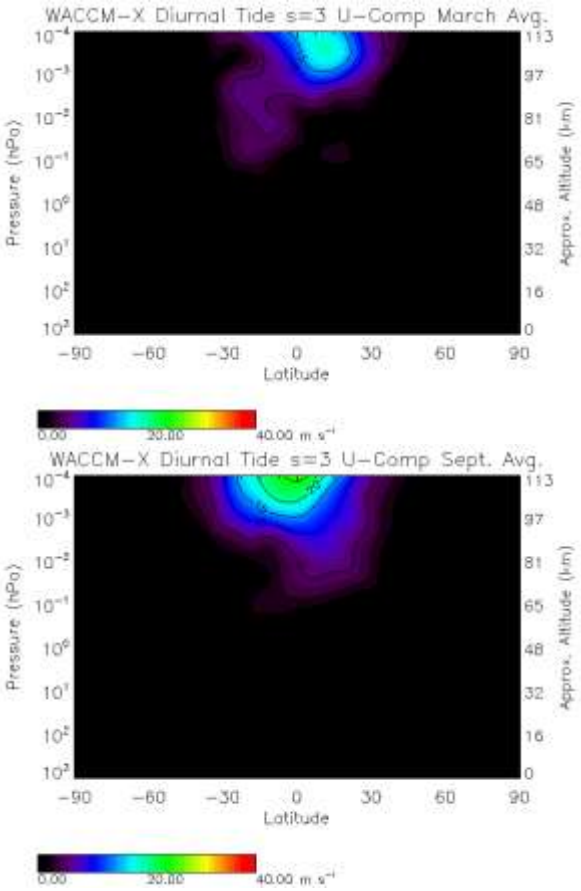
WACCM−X Diurnal Tide s=3 U−Comp March Avg.
Pressure (hPa)
Approx. Altitude (km)
Latitude
−90
−60
−30
0
30
60
90
0.00
20.00
40.00 m s⁻¹
WACCM−X Diurnal Tide s=3 U−Comp Sept. Avg.
Pressure (hPa)
Approx. Altitude (km)
Latitude
0.00
20.00
40.00 m s⁻¹

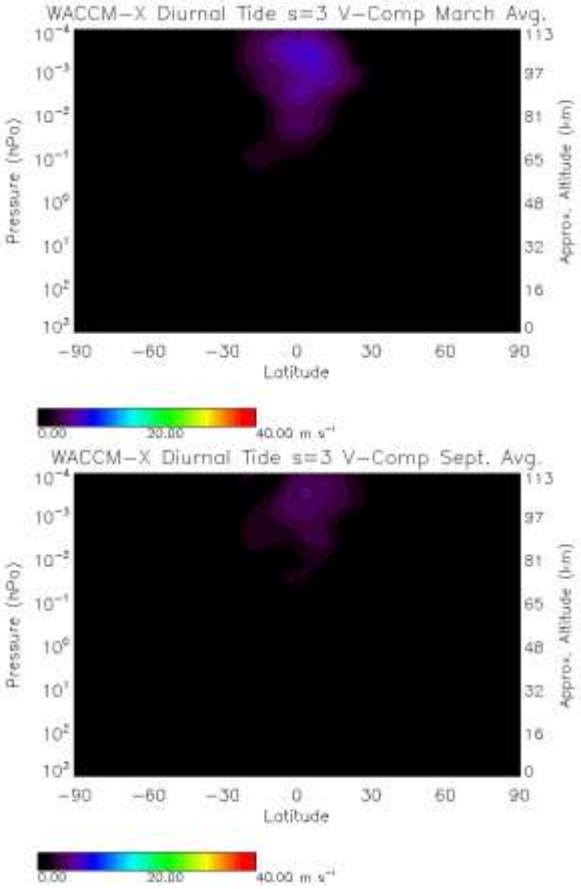
WACCM−X Diurnal Tide s=3 V−Comp March Avg.
Pressure (hPa)
Approx. Altitude (km)
Latitude
−90 −60 −30 0 30 60 90
0.00 20.00 40.00 m s⁻¹
WACCM−X Diurnal Tide s=3 V−Comp Sept. Avg.
Pressure (hPa)
Approx. Altitude (km)
Latitude
−90 −60 −30 0 30 60 90
0.00 20.00 40.00 m s⁻¹

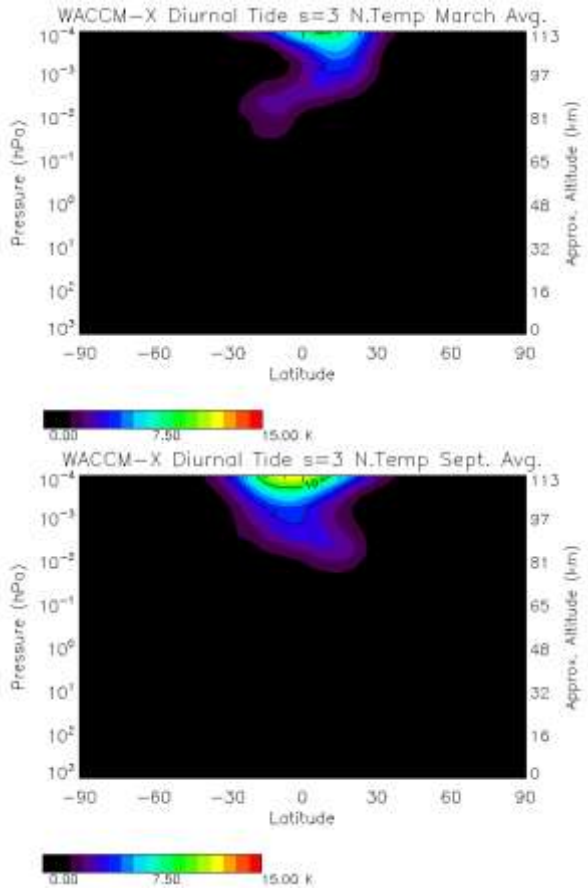

Figure 2. The DE3 monthly average amplitudes from March (left) and September (right) of the zonal wind (top), meridional wind (middle), and temperature (bottom). Wind contours of 5 m/s, temperature contours of 5 K.

2. The Whole Atmosphere Community Climate Model-Extended (WACCM-X)

[12] The Whole Atmosphere Community Climate Model-Extended (WACCM-X) [*Liu et al., manuscript in preparation,* 2009] is a three-dimensional, time-dependent comprehensive numerical model based on the software structure of the Whole Atmosphere Community Climate Model version 3 (WACCM3), which is in turn based on the NCAR Community Atmospheric Model version 3 (CAM3) [*Collins et al.,* 2004, *Garcia et al.,* 2007]. The WACCM-X utilizes the finite volume dynamical core from the CAM3, which calculates the mass fluxes into and out of a given volume, guaranteeing mass conservation. The governing equations of motion, physical parameterizations, and the numerical algorithms used in CAM3 are recorded in *Collins et al.* [2004] and http://www.ccsm.ucar.edu/models/atm-cam/docs/description; those of WACCM3 are documented in Garcia et al. [2007].

[13] To facilitate a three-dimensional representation of Earth's atmosphere up to 500 km, middle atmosphere chemistry and tracers are computed from the Model for Ozone and Related Tracers (MOZART), while mesospheric and lower thermosperic processes are adapted from the Thermosphere Ionosphere Mesosphere Electrodynamics General Circulation Model (TIME-GCM) [*Garcia et al.,* 2007, *Roble and Ridley,* 1994]. Thermospheric and ionospheric processes such as infrared (IR) cooling, auroral processes, ion drag, joule heating, molecular viscosity,

thermal diffusion, and parameterized gravity waves, among others, are included in the WACCM-X [*Liu et al.*, manuscript in preparation, 2009].

[14] WACCM-X is global model with 81 pressure levels extending over the entire altitude range of the model. The vertical coordinate system is comparable to that of the CAM3, which is purely isobaric above 100 mb and is a hybrid below that altitude [*Garcia et al.* 2007]. The vertical resolution varies with height: less than 1.0 km in the upper troposphere and lower stratosphere, 1-2 km in the stratosphere, and a half scale height in the upper atmosphere. The WACCM-X has a horizontal resolution of 1.9º x 2.5º (latitude x longitude) and a time step of 300 s.

[15] The WACCM-X produced three-hour output files from the one-year run of interest. These files contained parameter fields such as neutral temperature, zonal and meridional winds, concentrations of various molecular species, geopotential height, and vertical velocity (omega). Only neutral temperature, component winds, and omega fields were used in this study. Although these files were readily available, monthly averaged fields were computed for March and September to eliminate any day-to-day variability. These output fields were computed for medium solar activity, meaning the F10.7 solar radio flux was set to 144. This F10.7 flux serves as a satisfactory proxy of UV irradiance from the sun.

[16] Once these output files were obtained, spectral analysis was used to extract the tidal components of interest and plot them in the spectral space, as seen in Figures 1 and 2. Subsequently, a reverse Fourier transform was employed to reconstruct the neutral temperature, zonal, meridional, and vertical velocity fields associated with each tidal component. Figures 3 and 4 show reconstructed temperature, zonal, and meridional fields for the migrating diurnal tide and DE3 tide, respectively. Following this reconstruction, the EP Flux was computed to analyze the ways in which the different components interacted with the tropospheric and stratospheric source regions and the MLT dissipation region.

.

3. Eliassen-Palm Flux (EP Flux)

[17] Many middle/upper atmospheric processes can be analyzed by the interaction of the zonal-mean flow with perturbations that are superimposed upon it [*Andrews et al.* 1987]. The structure of the mean flow can alter the propagation of the diurnal tides, while these tides produce changes in momentum of the mean flow.

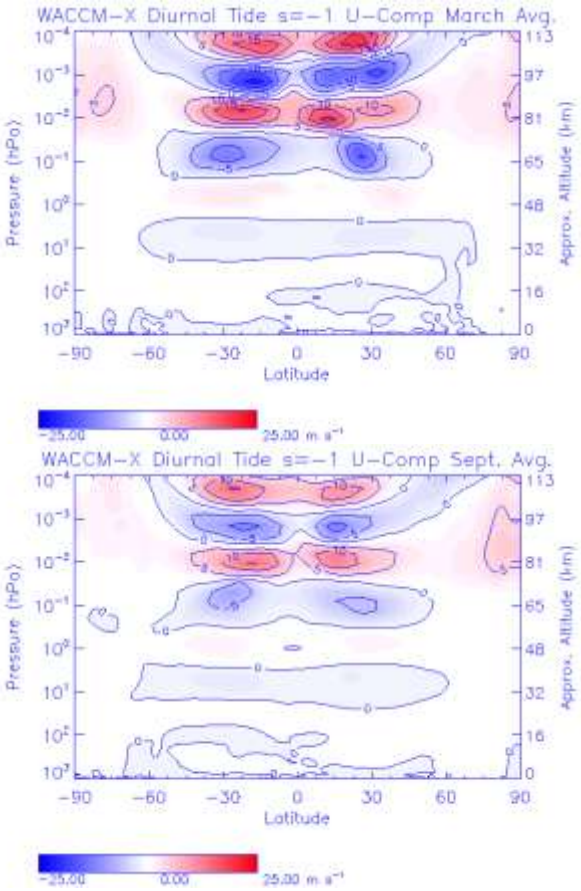
WACCM-X Diurnal Tide s=-1 U-Comp March Avg.
Pressure (hPa)
Approx. Altitude (km)
Latitude
-90
-60
-30
0
30
60
90
WACCM-X Diurnal Tide s=-1 U-Comp Sept. Avg.
Pressure (hPa)
Approx. Altitude (km)
Latitude
-25.00
0.00
25.00 m s⁻¹

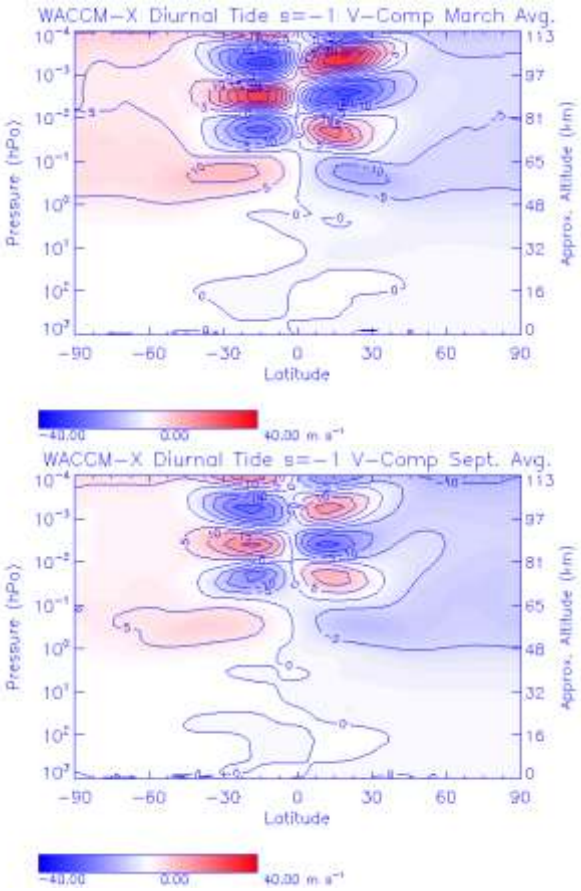
WACCM–X Diurnal Tide s=–1 V–Comp March Avg.
Pressure (hPa)
Approx. Altitude (km)
Latitude
WACCM–X Diurnal Tide s=–1 V–Comp Sept. Avg.
Pressure (hPa)
Approx. Altitude (km)
Latitude

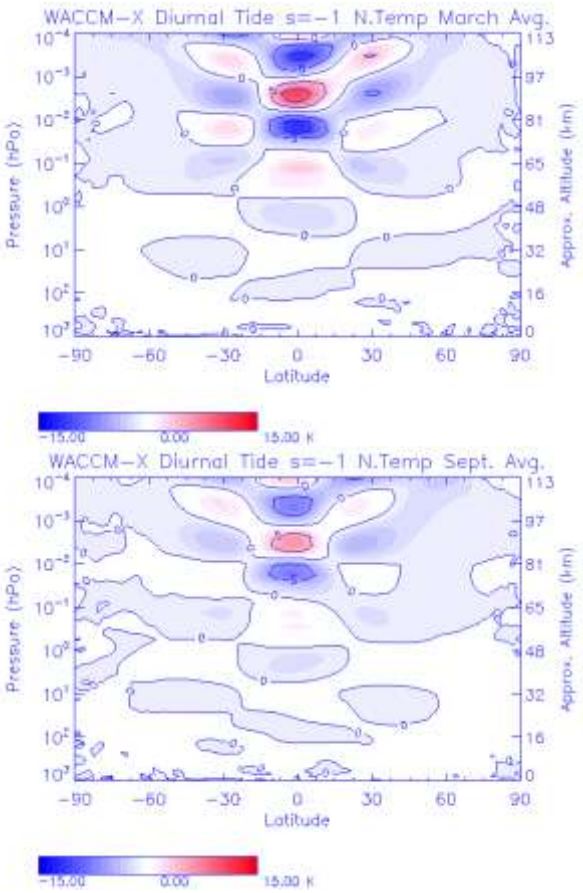

Figure 3. The migrating diurnal tide monthly average reconstructed fields from March (left) and September (right) of the zonal wind (top), meridional wind (middle), and temperature (bottom) at 0˚ longitude and 0 LT. Wind contours of 5 m/s, temperature contours of 5 K.

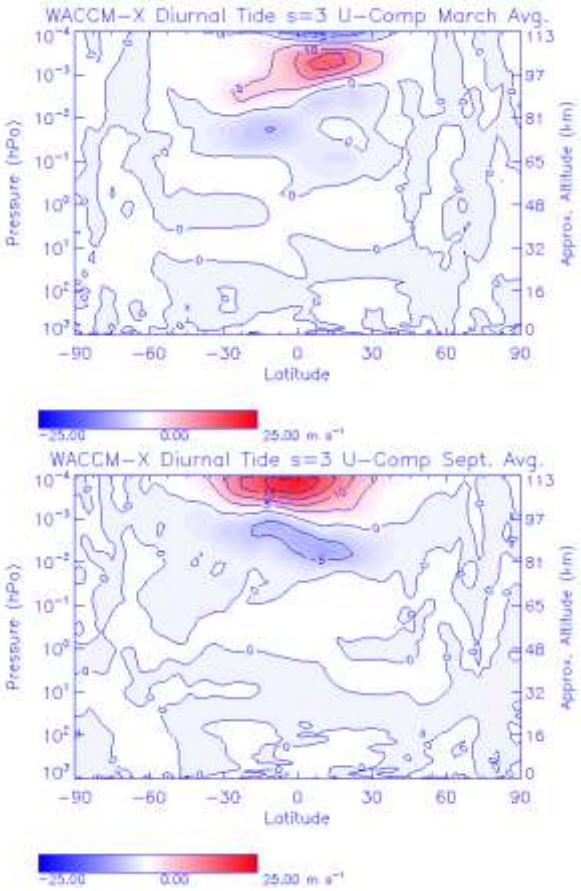
WACCM–X Diurnal Tide s=3 U–Comp March Avg.
Pressure (hPa)
Approx. Altitude (km)
Latitude
WACCM–X Diurnal Tide s=3 U–Comp Sept. Avg.
Pressure (hPa)
Approx. Altitude (km)
Latitude

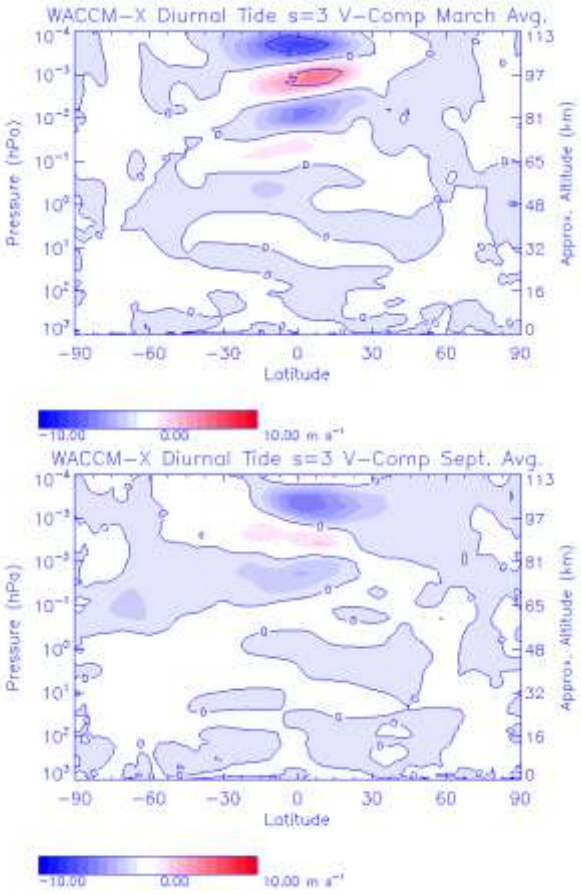
WACCM–X Diurnal Tide s=3 V–Comp March Avg.
Pressure (hPa)
Approx. Altitude (km)
Latitude
WACCM–X Diurnal Tide s=3 V–Comp Sept. Avg.
Pressure (hPa)
Approx. Altitude (km)
Latitude

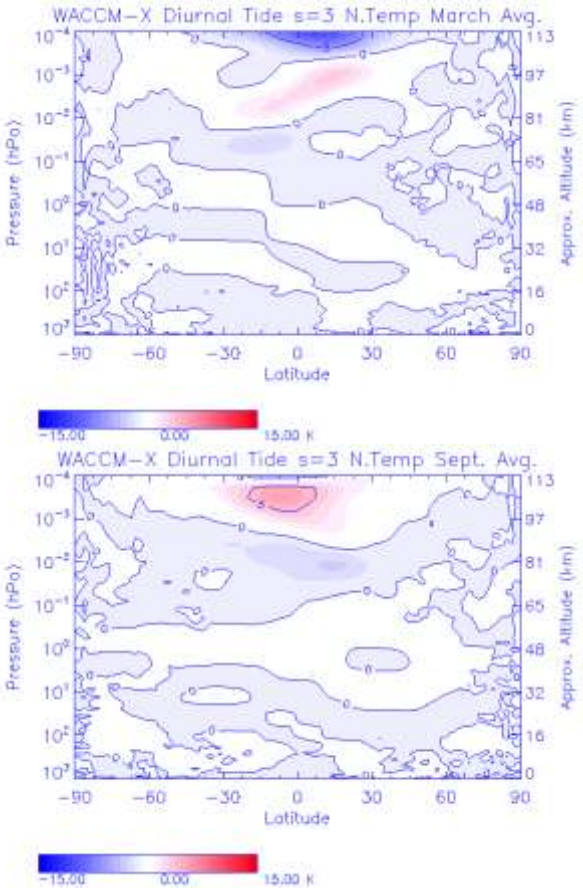

Figure 4. The DE3 monthly average reconstructed fields from March (left) and September (right) of the zonal wind (top), meridional wind (middle), and temperature (bottom) at 0˚ longitude and 0 LT. Wind contours of 5 m/s, temperature contours of 5 K.

As previously mentioned, atmospheric tides are dynamical perturbations that influence MLT structure; therefore employing a decomposition of atmospheric variables is a practical technique to use when diagnosing mean flow-tidal interaction. Previously, the EP Flux has been widely applied to analyze wave-mean flow interaction [e.g. *Lieberman,* 1998, *Edmon et al.,* 1980, *Mechoso et al.,* 1985, and *Hitchman et al.,* 1987]. The EP Flux serves as a generalized momentum flux and is therefore also a convenient formulation to use in this study of tidal sources and sinks of momentum throughout the troposphere, stratosphere and MLT region. The EP Flux arises after the governing equations of motion are decomposed into mean and disturbance quantities that are then Reynolds averaged, allowing us to isolate the effects perturbations have on the zonal mean flow. After further manipulation *Andrews et al.* [1987], the u-momentum equation in spherical coordinates is:

$$\overline{u_t} + \overline{v^*}\left[(a\cos\phi)^{-1}(\bar{u}\cos\phi)_\phi - f\right] + \overline{w^*}\overline{u_z} - \bar{X} = (\rho_0\, a\cos\phi)^{-1}\nabla\cdot\mathbf{F}, \tag{1}$$

where $\overline{v^*} \equiv \bar{v} - \rho_0^{-1}\left(\rho_0\overline{v'\theta'}/\bar{\theta}_z\right)_z$, (2)

and $\overline{w^*} \equiv \bar{w} + (a\cos\theta)^{-1}\left(\cos\phi\ \overline{v'\theta'}/\bar{\theta}_z\right)_\phi$. (3)

The vector **F** $\equiv$ (0, $F^{(\phi)}$, $F^{(z)}$) is the EP Flux; its components are given by:

$$F^{(\phi)} \equiv \rho_0 a \cos\theta \left(\bar{u}_z \overline{v'\theta'}/\bar{\theta}_z - \overline{v'u'}\right); \quad (4)$$

$$F^{(z)} \equiv \rho_0 a \cos\theta \left\{\left[f - (a\cos\theta)^{-1}(\bar{u}\cos\phi)_\phi\right]\overline{v'\theta'}/\theta_z - \overline{w'u'}\right\}, \quad (5)$$

where u is the zonal component of the wind, v is the meridional component of the wind, w is the vertical component of the wind, $\overline{v'u'}$ is the meridional flux of zonal momentum, $\overline{v'\theta'}$ is the meridional heat flux, and $\overline{w'u'}$ is the vertical flux of the zonal momentum. Other terms include potential temperature (θ), height (z), density (ρ_0), the radius of the earth (a), the Coriolis parameter (f), and latitude (ϕ). The over bar terms are mean quantities and the primed terms are perturbation quantities. The EP Flux acts as a forcing term in the u-momentum equation shown above. Calculating the individual components and divergence of the EP Flux provides the necessary quantitative measures to effectively identify tidal sources and sinks of momentum.[1] [18] Initially the pressure, density, potential temperature, and vertical velocity had to be calculated for every model grid point from the monthly averaged fields of March and September. The reconstructed neutral temperature and wind fields, along with the pressure, density, vertical velocity, and stability were used to compute the EP Flux components and divergence. For each tidal component of interest during the months of March and September, the EP Flux (**F**) and EP Flux tendency (ρ_0 $(a\cos\phi)^{-1}\nabla \cdot F$), are plotted for each tidal component of interest during the months of March and September.

4. The Migrating Diurnal Tide

[19] Figure 5 depicts the calculated EP Flux tendency within the troposphere-tropopause region during the months of March and September. A positive acceleration in the zonal mean flow (red) corresponds to a divergence of tidal momentum and thus represents a source of tidal momentum. Conversely, a deceleration in the zonal mean flow (blue) corresponds to a convergence of tidal momentum and therefore a dissipation of tidal momentum. Figure 5 begins calculating the EP Flux tendency at ~700 hPa due to the large variability in lower tropospheric processes (e.g. planetary boundary layer process).

[20] Both months show a source of tidal momentum in the summer hemisphere (i.e., the hemisphere coming out of summer), which extends throughout the lowest 8 km at tropical latitudes. The maximum acceleration in September (45.63 x 10^{-3} m s^{-1} day^{-1}) is greater than the maximum acceleration calculated during March (34.28 x 10^{-3} m s^{-1} day^{-1}). Figure 5 also displays a prominent dissipation region directly above the robust source region during both months. Exhibiting the same characteristics as those observed in the source regions with respect to latitude and hemispheric location, these dissipation regions stretch from ~8 km to ~15 km in both months. During March, there was a greater maximum transfer of tidal momentum to the zonal mean flow (-43.70 x 10^{-3} m s^{-1} day^{-1}), when compared to September (-30.81 x 10^{-3} m s^{-1} day^{-1}). Seeing as the source in September is stronger and the sink is weaker than those realized in March, these tropospheric sources and sinks of tidal momentum do not appear to be the central

[1] Since the EP Flux divergence contributes to the tendency of the zonal mean wind, we refer to it as the EP flux tendency.

cause of the seasonal variation in amplitude associated with the migrating diurnal tide. Source regions observed in March and September are thought to be caused by both latent heat release due to convective processes and absorption of IR radiation from water vapor, although these claims warrant additional investigation.

[21] Stratosphere-stratopause sources and sinks of tidal momentum are shown in Figure 6. The substantial source region observed at ~40 km extending to ~48 km in March and September are likely attributable to the absorption of UV solar radiation by stratospheric ozone. During both months, the source begins at equatorial latitudes and stretches into the mid-latitudes. Unlike the tropospheric sources and sinks of tidal momentum, the stratospheric source observed during March inflicts a greater acceleration of the zonal mean flow than the acceleration calculated in September. In March, the maximum acceleration is 336.41×10^{-3} m s^{-1} day^{-1}, whereas the maximum acceleration in September is 263.17×10^{-3} m s^{-1} day^{-1}. Hence, the disparity in stratospheric sources of tidal momentum may offer a possible explanation for the seasonal variability in the tidal amplitude.

[22] Figure 7 presents the monthly average EP Flux tendency in the MLT region during March and September. The EP Flux tendency calculated in March indicates two distinct source regions around 100 km altitude and +/- 30 latitude, possibly accounting for the aforementioned seasonal variation in the migrating diurnal tide. March also exhibits two large dissipation regions, implying that more westward momentum is deposited into the zonal mean flow. This is consistent with the stronger tidal amplitude in March, owing to the greater dissipation of tidal momentum in March. Moreover, greater dissipation of tidal momentum in March might offer additional support for stronger tidal forcing at lower altitudes as well as a more favorable wind structure throughout the atmosphere around the vernal equinox.

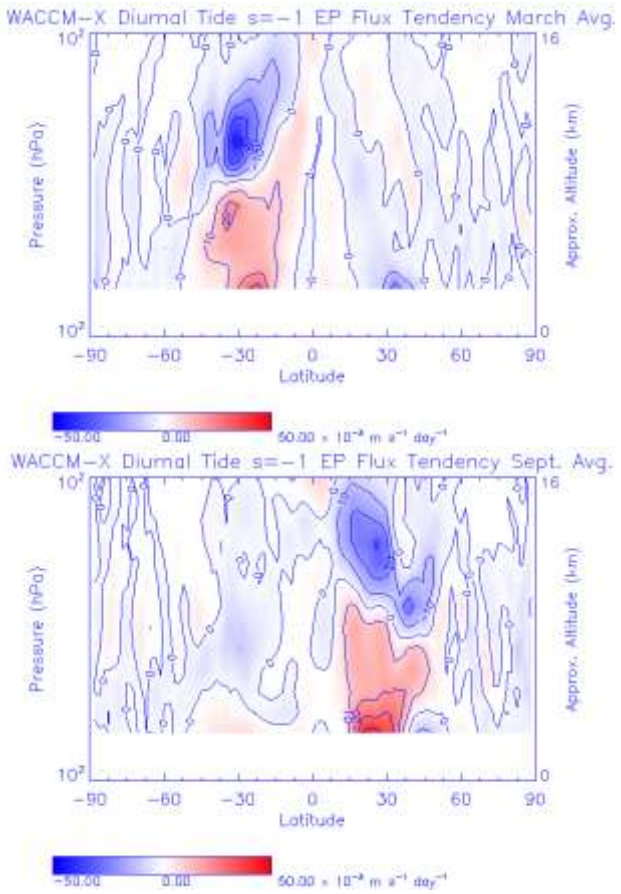

Figure 5. The migrating diurnal tide monthly averaged EP Flux tendency from March (left) and September (right) for the troposphere. EP Flux Tendency contours plotted every 10 m s^{-1} day^{-1}.

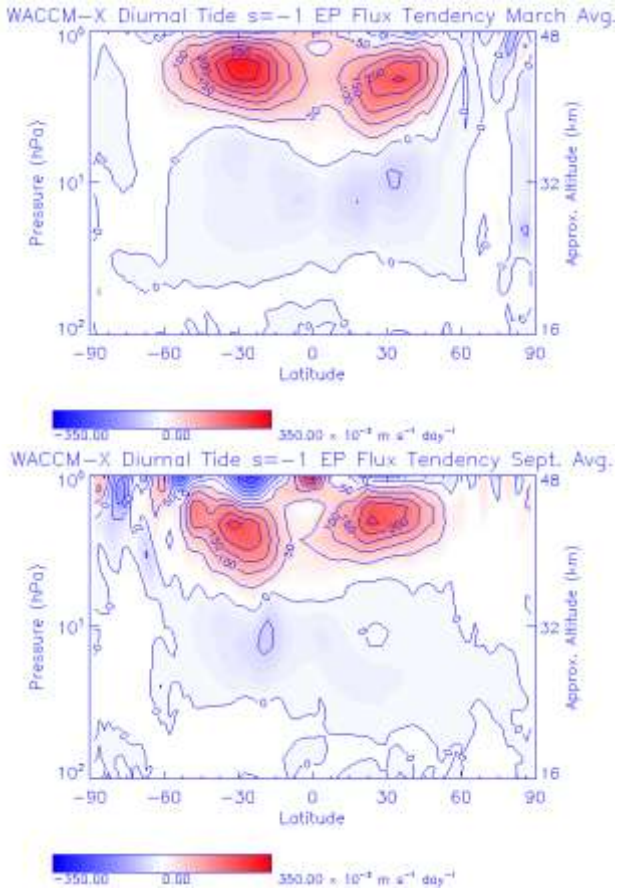

Figure 6. The migrating diurnal tide monthly averaged EP Flux tendency from March (left) and September (right) for the stratosphere. EP Flux Tendency contours plotted every 50 m s^{-1} day^{-1}.

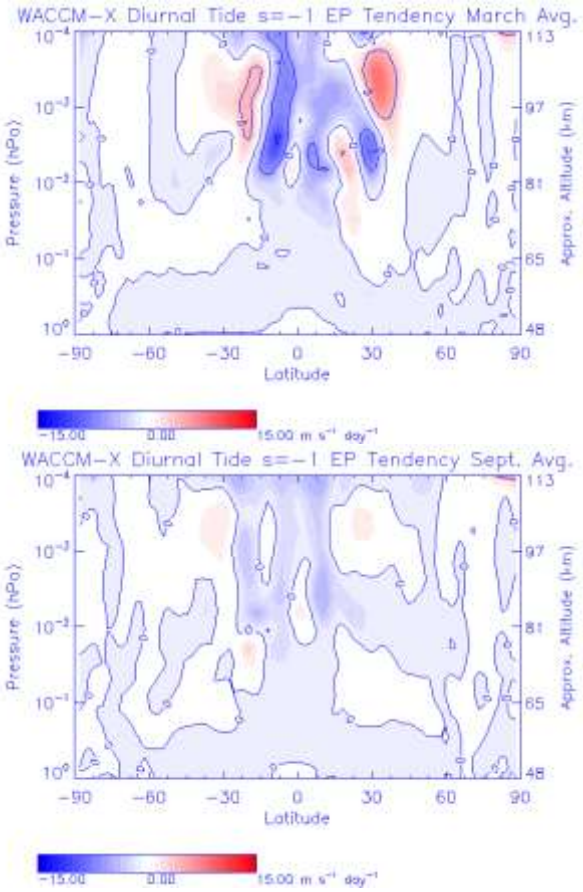

Figure 7. The migrating diurnal tide monthly averaged EP Flux tendency from March (left) and September (right) for the MLT. EP Flux Tendency contours plotted every 5 m s^{-1} day^{-1}.

5. The Diurnal Eastward 3 Tide (DE3)

[23] The EP Flux tendency of the DE3 tide throughout the troposphere is shown below in Figure 8. Because the DE3 propagates eastward and possesses eastward momentum, a negative acceleration represents a divergence of tidal momentum and thus a source region of tidal momentum. Conversely, a positive acceleration of the zonal mean flow corresponds to a convergence of tidal momentum and consequently a dissipation of tidal momentum. As with the migrating diurnal tide, we began calculating the EP Flux tendency at ~700 hPa, the considerable variability of the lower troposphere.

[24] The most striking features (Figure 8), consistent during both months, are the strong, anomalous generation and dissipation regions situated at high latitudes in the winter hemisphere. In March, the most likely explanation for the unusual region is computation error in the calculation of the EP Flux tendency at the northern boundary. During September, these source and dissipation regions extend further equatorward, suggesting that computational error might not provide the only explanation. Other explanations include nonlinear interactions with planetary waves, favorable polar jet stream characteristics over the one-year run, and instabilities associated with the polar jet stream. To solidify the above claims, further analysis is required.

[25] In Figure 8, both months reveal a similar source region located around the equator and at ~60˚ latitude in the summer hemisphere. Although these source regions are subtle, we

believe that latent heat release from deep convection may be responsible. With relative minimum acceleration values of -22.01×10^{-4} m s^{-1} day^{-1} and -29.27×10^{-4} m s^{-1} day^{-1}, calculated within the equatorial source in March and September respectively, seasonal variation is not apparent. In addition, relative minimum acceleration values of -29.02×10^{-4} m s^{-1} day^{-1} and -36.15×10^{-4} m s^{-1} day^{-1} in the mid-latitude source during March and September respectively, do not provide clear evidence of seasonal variation associated with the tidal sources.

[26] Continuing upward into the stratosphere-stratopause region (Figure 9), there is one noticeable generation region, located in the high latitudes of the southern hemisphere during September. This strong source region extends over the latitude range of ~60˚ S to ~82.5˚ S and over an altitude range of 8 km. Wind structure asymmetries in the southern hemisphere during September, when compared to those in the northern hemisphere during March, may offer a potential explanation. Increased instabilities and wind shear associated with the winter stratospheric jet could also account for this feature. Again, the cause of this source region warrants additional research efforts.

[27] Figure 10, below, displays the EP Flux tendency in the MLT region for the DE3 during March and September. The majority of the structure is contained within the highest 16 km of the MLT region, where strong dissipation of tidal momentum is occurring. A greater amount of momentum was exchanged with the background flow during September, as the magnitude of dissipation increases by approximately a factor of two. Furthermore, the structure of these dissipation regions reinforces the structure of tidal winds and temperature observed in Figure 2. This seasonal variation in dissipation regions may imply that during September, there are more favorable tidal propagation conditions, as well as greater tidal forcing from lower altitudes. This will be further investigated in future studies.

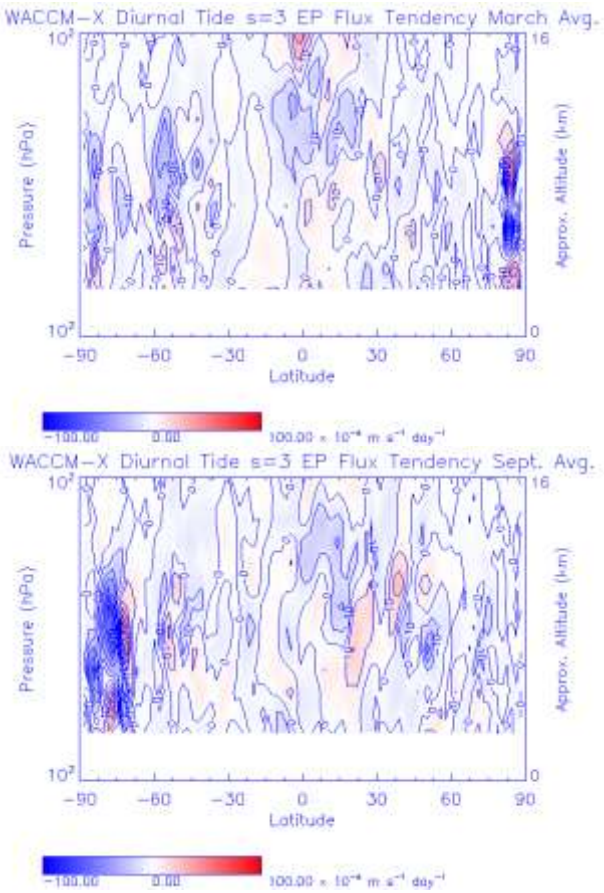

Figure 8. The DE3 monthly averaged EP Flux tendency from March (left) and September (right) for the MLT region. EP Flux Tendency contours plotted every 10 m s^{-1} day^{-1}.

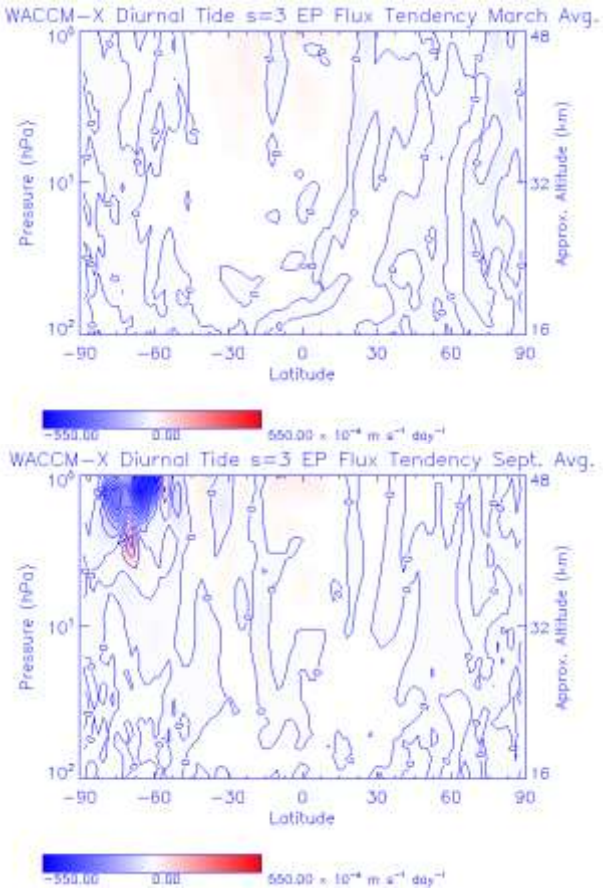

Figure 9. The DE3 monthly averaged EP Flux tendency from March (left) and September (right) for the stratosphere. EP Flux Tendency contours plotted every 10 m s^{-1} day^{-1}.

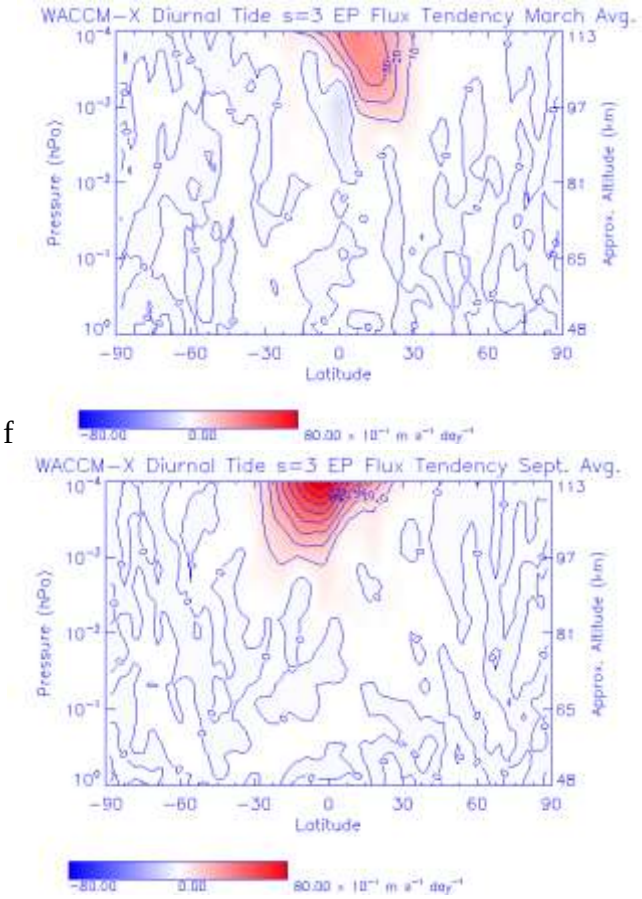

Figure 10. The DE3 monthly averaged EP Flux tendency from March (left) and September (right) for the MLT. EP Flux Tendency contours plotted every 10 m s^{-1} day^{-1}.

6. Summary and Conclusion

[28] The migrating diurnal tide and the DE3 tide are two tidal components that affect the dynamics and structure of the MLT and low-altitude ionosphere. Previous tidal analyses have documented semiannual variations in amplitudes associated with tidal perturbations in winds and temperature. Understanding the ways in which the migrating diurnal tide and the DE3 tide are seasonally generated and dissipated provides further knowledge of this semiannual variability. Calculating the EP Flux tendency from the WACCM-X allowed us to diagnose the ways in which these two tidal components dynamically interact with the zonal mean flow in the MLT region.

[29] In this model, tropospheric analyses of the migrating diurnal tide yielded two prominent source and dissipation regions of tidal momentum. However, distinct seasonal variation in these source and sink regions was not evident, as was predicted by *Hays et al.* [1994]. Differential ozone heating in the stratosphere during the months of March and September appears to offer the best explanation for the seasonal variability in amplitudes of the migrating diurnal tide. Stronger momentum exchange between the migrating diurnal tide and the zonal mean flow occurs during March in the MLT region, which reinforces the stronger zonal and meridional wind amplitudes depicted in Figure 1.

[30] Against conventional knowledge, varying tropospheric generation regions alone do not explain the seasonal variability in the tidal amplitude of the DE3 tide as analyzed in the WACCM-X. Within the stratosphere, the DE3 tide experienced one large generation region which could be attributed to the dynamics of the deteriorating stratospheric polar jet stream. MLT dissipation of DE3 tidal momentum proved to be greater during September than in March, partially corresponding to increased tidal winds at those altitudes.

[31] As a preliminary WACCM-X tidal analysis, this study has presented the groundwork necessary to begin substantiating the above diagnoses associated with the seasonal variability of the migrating diurnal tide and the DE3 tide. In particular, computing monthly averaged fields over the entire one-year run could prove useful in future diagnostic studies. Furthermore, determining ozone distribution and direct solar heating in the stratosphere and projecting those quantities onto the tidal modes may prove to be informative in describing the seasonal variability in ozone heating. Additional research into the stratospheric source of DE3 momentum during the month of September is essential to better comprehending the source region depicted at high southern latitudes. In summary, this initial diagnostic tidal analysis of the WACCM-X, provided better understanding of how and by what mechanisms the migrating diurnal tide and the DE3 tide are generated and dissipated by the background flow.

7. Acknowledgements

[32] Thank you to the SOARS® Staff and Protégés, the RESESS® Staff and Protégés, and all colleagues from the National Center for Atmospheric Research/High Altitude Observatory that not only contributed to this research, but to my future development in the sciences as well. A special thanks to my scientific mentors Han-Li Liu and Arthur Richmond, my writing and communications mentor Jamaica Jones, and my computer mentor Joe McInerney for all of your hard work and devotion in making this a productive and enlightening summer. Additionally, a special thanks goes out to Ben Foster, Jeff Forbes, Stan Solomon, and the IT Staff at the High Altitude Observatory for their assistance on this project.

References:

American Meteorological Society (2008), SPACE WEATHER A Policy Statement of the American Meteorological Society, *Bulletin of the American Meteorological Society*, *89*, (6), 16-18.

Andrews, D. G., J. R. Holton, C. B. Leovy (1987), *Middle atmosphere dynamics*, *International Geophys. Ser.*, vol. 40, edited by R. Dmowska and J. R. Holton, pp. 487, Academic Press, Inc.

Chapman, S., and R.S. Lindzen (1970), *Atmospheric Tides*, Gordon and Breach, New York.

Chang, L., S. Palo, M. Hagan, J, Richter, R. Garcia, D. Riggins, D. Fritts (2008), Structure of the migrating diurnal tide in the Whole Atmosphere Community Climate Model (WACCM), *Advances in Space Research*, *41*, 1398-1407.

Collins, W. D., et al. (2004), Description of the NCAR Community Atmosphere Model (CAM3), Natl. Center for Atmos. Res., Boulder, Colo.

Coster, A. and A. Komjathy (2008), Space Weather and the Global Positioning System, *Space Weather, 6*, S06D04, doi: 10.1029/2008SW000400.f.

Dabas, S. R. (2000), Ionosphere and its Influence on Radio Communication, *Journal of Science Education*, *5*, 28 – 43.

Edmon, H., B. Hoskins, and M. McIntyre, 1980: Eliassen-Palm Cross Sections for the Troposphere. *J. Atmos. Sci.*, *37*, 2600–2616.

Forbes, J. M. (1995), Tidal and planetary waves, in The Upper Mesosphere and Lower Thermosphere: A Review of Experiment and Theory, *Geophys. Monogr. Ser.*, *vol. 87*, edited by R. M. Johnson and T. L. Killeen, pp. 67– 87, AGU, Washington, D. C.

Garcia, R. R., D. R. Marsh, D. E. Kinnison, B. A. Boville, and F. Sassi (2007), Simulation of secular trends in the middle atmosphere, 1950–2003, *J. Geophys. Res.*, *112*, D09301, doi:10.1029/2006JD007485.

Hagan, M. E., R. G. Roble, and J. Hackney (2001), Migrating thermospheric tides, *J. Geophys. Res., 106*, *12*,739– 12,752.

Hagan, M. E., and J. M. Forbes (2002), Migrating and nonmigrating diurnal tides in the middle and upper atmosphere excited by tropospheric latent heat release, J. Geophys. Res., 107(D24), 4754, doi:10.1029/2001JD001236.

Hagan, M. E., and J. M. Forbes (2003), Migrating and nonmigrating semidiurnal tides in the upper atmosphere excited by tropospheric latent heat release, J. Geophys. Res., 108(A2), 1062, doi:10.1029/2002JA009466.

Hays, P.B., D.L. Wu, and T. HRDI Science Team, (1994), Observations of the Diurnal Tide from Space. *J. Atmos. Sci., 51*, 3077–3093.

Hitchman, M.H., C.B. Leovy, J.C. Gille, and P.L. Bailey, 1987: Quasi-Stationary Zonally Asymmetric Circulations in the Equatorial Lower Mesosphere. *J. Atmos. Sci., 44*, 2219–2236.

Kelley, M. C. (1989), *The Earth's Ionosphere- Plasma Physics and Electrodynamics, International Geophys. Ser.*, vol. *40* edited by R. Dmowska and J.R. Holton, Academic Press, San Diego.

Lieberman, R.S., 1999: Eliassen–Palm Fluxes of the 2-Day Wave. *J. Atmos. Sci., 56*, 2846–2861.

Liu, H. -L., B. T. Foster, R. R. Garcia, M. E. Hagan, D. E. Kinnison, J. M. McInerney, D. R. Marsh, A. Maute, L. Qian, A. D. Richmond, J. H., Richter, R. G. Roble, Fabrizio Sassi, A. K. Smith, and S. C. Solomon, Thermosphere and Ionosphere Extension of the Whole Atmosphere Community Climate Model (WACCM-X), in preparation.

Maeda, H. (1968), Variation in geomagnetic field, *Space Sci. Rev., 8*, 555-590.

Mechoso, C.R., D.L. Hartmann, and J.D. Farrara, 1985: Climatology and Interannual Variability of Wave, Mean-Flow Interaction in the Southern Hemisphere. *J. Atmos. Sci., 42*, 2189–2206.

Pancheva, D., P. Mukhtarov, and B. Andonov (2009), Global structure, seasonal and interannual variability of the migrating semidiurnal tide seen in the SABER/TIMED temperatures (2002-2007), *Ann. Geophys., 27*, 687-703.

Richmond, A.D (1995), *Ionospheric electrodynamics, in Handbook of Atmospheric Electrodynamics*, Vol. II (H. Volland, ed.), CRC Press, Boca Raton, Florida, 249-290.

Richmond, A.D., and R.G. Roble (1987), Electrodynamic effects of thermospheric winds from the NCAR thermospheric general circulation model, *J. Geophys. Res., 92*, 12,365-12,376.

Roble, R.G., and E.C. Ridley (1994), A thermosphere-ionosphere-mesosphere-electrodynamics general circulation model (time-GCM): equinox solar cycle minimum simulations (30-500 km), *Geophys. Res. Lett., 21*, 417-420.

Vincent, R. A., T. Tsuda, and S. Kato, (1989), Asymmetries in mesospheric tidal structure, *Journal of Atmospheric and Terrestrial Physics*, *51,* 609-616.

Volland, H. (1988), *Atmospheric Tidal and Planetary Waves*, pp. 348, Kluwer Academic Publishers, Dordrecht, The Netherlands.

Wu, Q., D. A. Ortland, T. L. Killeen, R. G. Roble, M. E. Hagan, H.-L. Liu, S. C. Solomon, J. Xu, W. R. Skinner, and R. J. Niciejewski (2008), Global distribution and interannual variations of mesospheric and lower thermospheric neutral wind diurnal tide: 1. Migrating tide, *J. Geophys. Res.*, 113, A05308, doi:10.1029/2007JA012542.

Wu, Q., D. A. Ortland, T. L. Killeen, R. G. Roble, M. E. Hagan, H.-L. Liu, S. C. Solomon, J. Xu, W. R. Skinner, and R. J. Niciejewski (2008), Global distribution and interannual variations of mesospheric and lower thermospheric neutral wind diurnal tide: 2. Nonmigrating tide, *J. Geophys. Res.*, 113, A05309, doi:10.1029/2007JA012543.